

SAFE CONTROL OF MANUFACTURING VEHICLES RESEARCH TOWARDS STANDARD TEST METHODS

Roger Bostelman, Will Shackelford, Geraldine Cheok, Kamel Saidi

**National Institute of Standards and Technology
100 Bureau Drive, Stop 8230
Gaithersburg, MD 20899**

Abstract

The National Institute of Standards and Technology's Intelligent Systems Division has been researching several areas leading to safe control of manufacturing vehicles to improve automated guided vehicle (AGV) safety standards. The research areas include:

- AGV safety and control based on advanced two-dimensional (2D) sensors that detect moving standard test pieces representing humans;
- Ability of advanced 3D imaging sensors, when mounted to an AGV or forklift, to detect stationary or moving objects and test pieces on the ground or hanging over the work area; and
- Manned forklift safety based on advanced 3D imaging sensors that detect visible and non-visible regions for forklift operators.

Experiments and results in the above areas are presented in this paper. The experimental results will be used to develop and recommend standard test methods, some of which are proposed in this paper, and to improve the standard stopping distance exception language and operator blind spot language in AGV standards.

1 Introduction

The Mobile Autonomous Vehicles for Manufacturing (MAVM) Project at the National Institute of Standards and Technology (NIST) has been researching methods to improve safety standards for automated guided vehicles (AGV), automated functions for manned powered industrial vehicles, and forklift operator visibility. Specifically, members of the MAVM Project have been involved in:

- the American National Standards Institute/Industrial Truck Standards Development Foundation (ANSI/ITSDF) B56.5-2005 Safety Standard for Guided Industrial Vehicles and Automated Functions of Manned Industrial Vehicles and
- the ANSI/ITSDF B56.11.6-2005 Evaluation of Visibility From Powered Industrial Trucks.

The ANSI/ITSDF B56.5 standard “defines the safety requirements relating to the elements of design, operation, and maintenance of powered, not mechanically restrained, unmanned automatic guided industrial vehicles and automated functions of manned industrial vehicles.” [1]

ANSI/ITSDF B56.11.6 “establishes the conditions, procedures, equipment and acceptability criteria for evaluating visibility from powered industrial trucks.” [2] The MAVM Project has addressed specific areas of these two standards by developing test methods that could potentially lead to improving these standards and to provide safe control of manufacturing vehicles.

Background NIST involvement in ANSI/ITSDF B56.5

In 2010, NIST suggested improvements to the B56.5 standard including a new test piece, test piece coatings, and non-contact sensor and vehicle performance requirements for detecting static test pieces in the vehicle path. The committee voted to accept the improvements and the standard was revised and published. However, the standard still includes an exception for obstacles suddenly appearing at less than the minimum AGV stopping distance. The exception states: “Although the vehicle braking system may be performing correctly and as designed, it cannot be expected to function as designed should an object suddenly appear in the path of the vehicle and within the designed safe stopping distance. Examples include, but are not limited to, an object falling from overhead or a pedestrian stepping into the path of a vehicle at the last instant.” [1] The term “safe stopping distance” refers to the distance between the leading edge of the sensing field and the vehicle structure. For this paper, the B56.5 ‘exception zone’ on the AGV will be called the ‘stop zone’ which is typically the label given to this programmed area for current safety sensors.

To support the 2010 B56.5 improvements, NIST performed experiments using 3D imaging sensors to detect static test pieces in the AGV path. NIST researchers then reviewed the data and subjectively considered whether or not the test piece was detected appropriately by the sensor (i.e., if there were compelling data demonstrating that a test piece was detected). The experiments demonstrated that static test pieces could be detected using current 2D and advanced 3D imaging sensors mounted to a static AGV [3]. However, to prove that detection is possible in a real system, a computer algorithm would need to be developed to detect test pieces and provide the appropriate slow or stop command to the AGV.

In experiments conducted in 2011 and 2012, NIST researchers used 2D and 3D imaging sensors mounted to an AGV. In contrast to the 2010 experiments where the test piece was static, in these experiments the AGV and the test piece were both moving. The test piece entering the AGV path was detected by the sensors and the distance of the test piece to the AGV was calculated and analyzed. Two different test methods were used to measure the dynamic test piece distance from a dynamic AGV: 1) AGV navigation and control data were compared to ground truth and 2) a generic video and grid method using no AGV navigation information was compared to ground truth. Method 1 experimental setup, data collection, software and results are detailed in [4] and results are briefly described in this paper. Method 2 experiments and results are detailed in this paper. Additionally, 3D imaging sensor data were collected and are described and shown in this paper. 3D imaging appears to be useful for detecting both static and dynamic and ground-based and overhanging obstacles. Future experiments to incorporate 3D imaging

data to implement slowing and stopping control for AGVs are planned. As a start, NIST has attached 3D imaging sensors to forklifts where sensor data were input to software algorithms that control alert lights. The forklift alerts experiment is further described in this paper.

Background NIST support for ANSI/ITSDF B56.11.6

A large number (80 %) of forklift accidents involve pedestrians. Such accidents occur on average once every three days [5]. The B56.11.6 standard allows up to 20 % of the regions surrounding a forklift to be obscured from the operator. Nonetheless, operators are typically declared at fault for the accidents. B56.5 and several other standards are based on B56.11.6. The MAVM Project has been researching forklift safety [6] [7] because forklift accident rates are so high and B56.5 includes manned forklifts with automated functions. Onboard sensors integrated with semi-autonomous vehicle control can detect obscured regions and may improve safety. However, B56.11.6 measurement methods provide only information about how much of the area is not visible to the operator. Advanced operator visibility measurement technology and methods could potentially map obscured regions, as well as suggest optimal sensor mounting locations and the fields of view (FOV) needed to detect obstacles in obscured regions.

The MAVM Project is exploring the use of advanced visibility measurement technology for manned industrial vehicles to improve standard test methods. This paper provides preliminary test and analysis methods for advanced operator visibility measurement. The experimental results provided here will be used to help develop further tests and standard test methods for inclusion in AGV standards, as well as to develop improved standard stopping distance exception language. This paper also includes preliminary operator visibility tests and proposed test methods for using advanced technology with an explanation of how the technology can provide required standard results. Results and conclusions are also presented.

2 Dynamic Experiments

Two different test methods, 1 and 2, were implemented for detecting when a dynamic test piece entered the path of a moving AGV within the AGV stop zone. Test Method 1 used AGV navigation and control data compared to ground truth. Method 1 results and issues are briefly discussed in section 2.1 and are detailed in [4]. Test Method 2 used an alternative, generic, video-grid method using no AGV navigation information and was also compared to ground truth. Method 2 is detailed in section 2.2.

2.1 Method 1 Dynamic Experiments and Results

Several sensors were mounted to the NIST AGV, as shown in Figure 1¹. The AGV was programmed to move in a straight line to a chosen navigational point. Both two- and

¹ Certain trade names and company products are mentioned in the text or identified in an illustration in order to adequately specify the experimental procedure and equipment used. In no case does such an

three-dimensional (2D and 3D) sensors were used to collect data, including: a color camera, an infrared camera, two different types of 3D light detection and ranging (LIDAR) sensors and two 2D line-scanning laser detection and ranging (LADAR) sensors, mounted horizontally and vertically where one was a safety rated sensor. The safety sensor was mounted to scan horizontally at a height of 10 cm above the floor. It is a sensor typically used in industry as a non-contact safety sensor for AGVs. The data from the 3D imaging sensors will be used in future efforts to research their effectiveness at detecting obstacles, especially overhanging obstacles discussed in section 4 of this paper. The safety sensor data, collected simultaneously with the 3D sensor data, were used for dynamic obstacle detection and for AGV control. The safety sensor was used to detect ground-based obstacles.

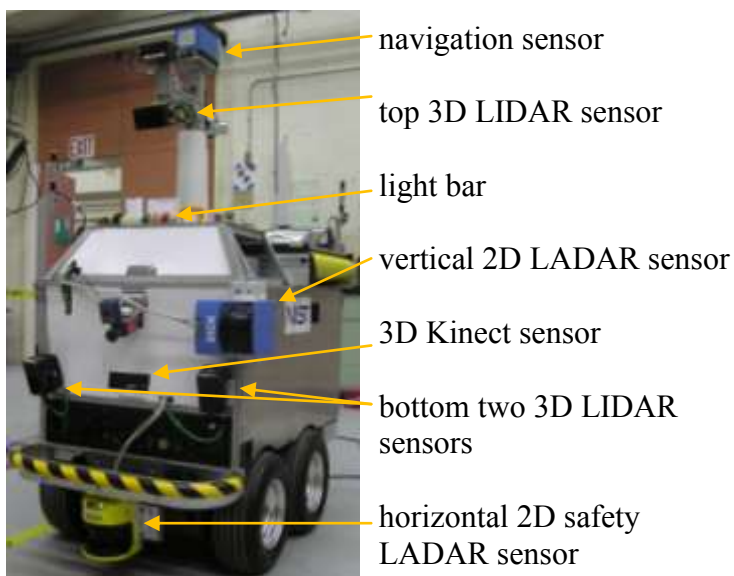


Figure 1 – NIST AGV

Two types of ‘AGV stop’ control tests were performed: controlled braking and low-level emergency stop (e-stop) control.

B56.5 states that “Controlled braking may be provided” and is “a means for an orderly slowing or stopping of the vehicle.” Controlled braking was used to demonstrate continuous AGV control to reduce AGV energy upon detection of an

obstacle within the programmed AGV path and

at any range within the detection limit of the safety sensor. B56.5 states that “Emergency braking shall be provided for all vehicles. The emergency brake shall be mechanically set and require power or force from a source external to the brake to release.” In the case of the NIST AGV, there is no mechanical brake and instead, the vehicle coasts to a stop when the safety sensor detects an obstacle in the AGV path and while in the mode we call “low-level emergency stop (e-stop) control.” However, the NIST AGV integrates the safety sensor directly into the AGV drive amplifiers, which is typical of industrial AGV’s, and must use an electrical reset from a wireless safety system to externally reset the AGV to drive after an e-stop.

A sled was designed and built to repeatably move the B56.5 standard test pieces across the AGV path and within the AGV exception zone (see Figure 2). A modular,

identification imply recommendation or endorsement by the National Institute of Standards and Technology, nor does it imply that the products are necessarily the best available for the purpose.

laser-based measurement system with 250 μm accuracy was used to measure the ground truth locations of the sled and AGV. [8] The sled was pulled using a winch that began motion when the AGV tripped a tape switch on the floor. The tape switch positions were chosen so that the test piece entered and passed through the programmed safety sensor stop zone before the AGV could strike the sled components. The stop zone measured 2 m along the AGV path by 0.8 m wide. Open and confined spaces were other parameters in the NIST experiments.

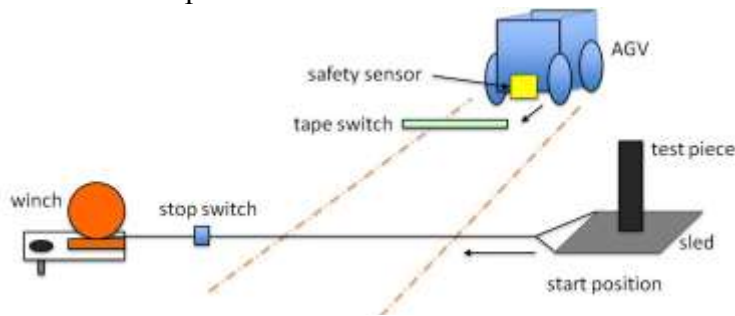


Figure 2 – Test setup showing the AGV, path, and test piece sled.

Method 1 experimental results showed an average of a 0.5 m measured difference between the onboard navigation AGV position and safety sensor test piece detection positions and the ground truth for the AGV and test piece positions. These results showed that the test pieces may or may not have been in the exception zone when they were detected. If the test piece was detected in front of the exception zone, the AGV was required to stop according to the B56.5 standard and therefore, the results could not be used in the exception zone test results. Low-level, emergency braking tests were performed and used to demonstrate that low-level, emergency braking can reduce the AGV's kinetic energy when test pieces are within the AGVs exception zone and can also control an AGV stop. However, the stop position always occurred beyond the test piece path indicating that the test piece would have been struck. Controlled braking tests were also performed and demonstrated that once the test piece entered the AGV path within the stop zone, the AGV decelerated to a stop faster than using only the emergency braking, where the vehicle coasted to a stop.

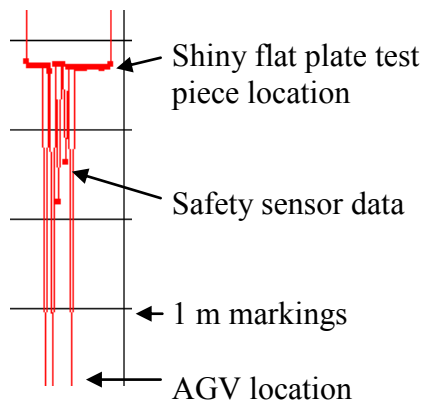


Figure 3 – Data from the safety sensor when mounted on the AGV and moving towards the shiny flat plate test piece.

More details are provided in reference [4], which describes potential sources of experimental errors. Also, there was a lot of noise in the data from the safety sensor. Therefore, there could be an error of up to ± 250 mm, depending on which point in this cloud was selected by the algorithm as the location at which the test piece first entered the AGV path. Previous experiments using highly reflective test pieces that were detected by a light-emitting sensor instead of a laser range scanner showed similar results. [9]

Figure 3 shows data collected from the safety sensor for a static, shiny flat plate in the

AGV path. As the AGV attempted to move towards the plate, it repeatedly stopped and started due to “spikes” in the data. Figure 3 shows the distances between the AGV and the plate. The spikes in the data are instances that caused the AGV's controller to determine that the plate is much closer than it actually is, causing it to stop.

The sensor and AGV industries are aware of this phenomenon and provided the following reason for it: Reflectors and very bright light blind the safety sensor because the light source emits infrared energy at the same frequency as the infrared of the safety sensor. The safety sensor follows UL 61496 Electro-Sensitive Protective Equipment [10] and EN 61496 [11]. These standards require the sensor to shut down for highly reflective surfaces. The industry also says that to correct the situation, the sensor should be angled to reflect light away from the source or, if possible, the reflective surface should be dulled.

2.2 Method 2 Dynamic Experiments

Method 2 is a more generic test method than Method 1 and is meant to be applied to any AGV or semi-autonomous forklift that may or may not have navigation or scanning LADAR sensing and therefore, provides measurement without requiring information from the vehicle. Method 2 is detailed in the following sub-sections.

2.2.1 Method 2 Experimental Setup

Test Method 2 used a printed grid on paper taped to the floor in the AGV path within the same test spaces used in Method 1. The grid was 4 m (L) x 1 m (W) and was divided into 20 cm segments marked with bold lines. These 20 cm segments were further subdivided into 5 cm sections marked with lighter lines. The grid was labeled every 1 m. For each 1 m x 1 m square, diagonal lines were drawn from the corners to provide additional location information and for easy review of particular squares (see Figure 8).

The 70 mm diameter x 400 mm tall vertical cylinder test piece was mounted on a short cart with wheels, which was used to push the test piece into the AGV path. For Method 2, a change was also made to stop the test piece in the AGV path instead of passing it through the path. This ensured that the test piece simulated a pedestrian or obstacle that was definitely in danger of being hit by the AGV. A video camera was mounted in the laboratory ceiling to capture the end of the AGV path where the AGV would slow or stop. However, the camera could have been placed anywhere where it could capture the entire test space (approximately 4 m wide) if it had a high enough resolution to clearly view the 5 cm or smaller grid blocks. At the start position, a photosensor, Photosensor 1, was placed on the floor next to the AGV so that the emitted laser beam was along the edge of the AGV stop zone. The emitted beam was reflected back to the photosensor by a reflector placed beyond the AGV stop zone. Although not used in the analysis, the onboard safety sensor data were also collected to determine when it detected the test piece entering the stop zone. Detection occurred when a yellow light, that was connected to the safety sensor and onboard the AGV, turned off. The researchers used the safety sensor detection to ensure that the photosensor was properly placed along the edge of the stop zone. The two sensors are not continuously aligned

during dynamic tests since the AGV moves from side to side by approximately 10 cm in some tests when heading to the end waypoint. However, photosensor and safety sensor detection times are typically within a few hundredths of a second of each other. The AGV, traveling at 1 m/s, moves at most 5 cm within this time. Photosensor 1 tripped a light that was pointed towards the video camera. The light turned off once the test piece crossed the beam.

Similarly, the beam from a second photosensor, Photosensor 2, crossed the AGV path to detect the approaching AGV and was used to turn on a second light. It was placed 1 m from the point where the test piece was pushed into the path. The 1 m distance was chosen to ensure that the test piece would be struck when the AGV traveled at 1 m/s and was well within the vehicle stop zone and distance at this speed. When the Photosensor 2 light turned on, the test piece was pushed into the path with a long bar. The person pushing the cart attempted to stop it in the AGV path.

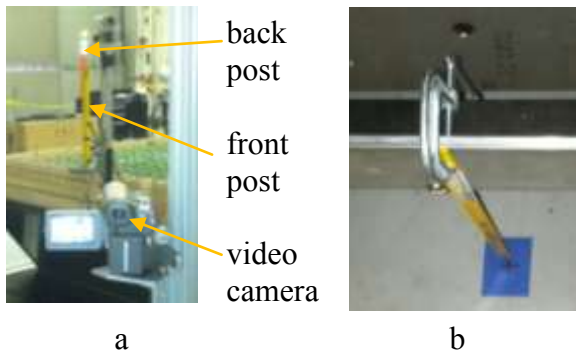


Figure 4 – AGV start point calibration setup showing: (a) aligned posts within the onboard camera FOV and (b) clamped bar on the AGV rear bumper pointing down to a start point on the floor.

For different experiments, the AGV was programmed to travel at 0.5 m/s, 1 m/s, or 2 m/s along a straight line and to stop at a waypoint approximately 10 m from the start point. To ensure that the AGV was positioned at a repeatable start location, a calibration method was used that made use of a video camera mounted to the vehicle. Figure 4 shows the AGV start point calibration setup. Two posts were set at approximately 5 m and 10 m along a line at an angle from the AGV so that when the AGV is at the start location, the two posts are aligned in the camera's field of view (FOV). Also, a thin bar was clamped to the rear AGV bumper pointing

down to a spot marked on the floor. This ensured that the vehicle was positioned at the same start point while the camera/post setup was used to ensure proper vehicle orientation.

Ground truth was captured for Test Method 2 experiments using the same measurement system as in Method 1. The ground truth system was used to track the AGV position during the experiments. It was also used to measure several points on the paper grid so that the positions obtained from the video images could be registered to the ground truth coordinate frame. Post processing was then used to analyze the validity of the grid method as compared to ground truth.

Test Method 2 experiments included three researchers: one to set up and start the AGV, one to push the test piece into the vehicle path, and one to begin the video and ground truth systems. One or two people would normally be required for manufacturers to implement Test Method 2 with their AGV.

2.2.2 Method 2 Data Collection

Video data were collected for Test Method 2 experiments to capture the Photosensor 1 light change, the onboard safety sensor detect light change, the test piece motion and stop location, and the AGV motion and stop position. The video replay capability had to allow frame-by-frame review of the experiment to gain approximate location information of the test piece and AGV. Figure 5 shows snapshots from the overhead video of Test 18 including when: (a) the test piece crosses Photosensor 1, (b) the test piece is detected by the AGV safety sensor, (c) the AGV hits the test piece (or when the test piece stops in the AGV path), (d) the AGV stops.

In Figure 5 d, the test piece is shown beneath the vehicle and in front of the wheel. The test piece was never run over by the AGV. A front shroud could be added to the AGV so that the test piece always stays in front of it.



Figure 5 – Snapshots from the overhead video showing when: (a) the test piece crosses the photo-sensor, (b) the test piece is detected by the AGV safety sensor, (c) the AGV hits the test piece (or when the test piece stops in the AGV path), (d) the AGV stops.

Using Figure 5, Test 18, as an example, the video shows that: at time 15:12, the test piece crossed the Photosensor 1 line; at time 15:14, the test piece was detected by the

AGV safety sensor; at time 15:28, the test piece was hit by the AGV and therefore the test piece stopped moving across the AGV path; and at 17:28, the AGV stopped.

2.2.3 Method 2 Grid Test Results

Figure 6 shows the AGV and test piece positions for each of the Figure 6 images, used to determine the decrease in energy from the AGV where:

- $d1$ = distance between the AGV and test piece when the test piece first enters the exception/stop zone as measured by the Photosensor 1. This number is slightly different from the point when the test piece is first detected by the AGV safety sensor. For these experiments, the location where the test piece was first detected by the safety sensor was ignored.
- $d2$ = the distance between the location where the test piece first enters the stop zone as measured by the Photosensor 1 and where the AGV stops.
- $d3$ = the distance between $d2$ and $d1$ i.e., the deceleration distance – used to show a reduction in AGV energy applied to the test piece.

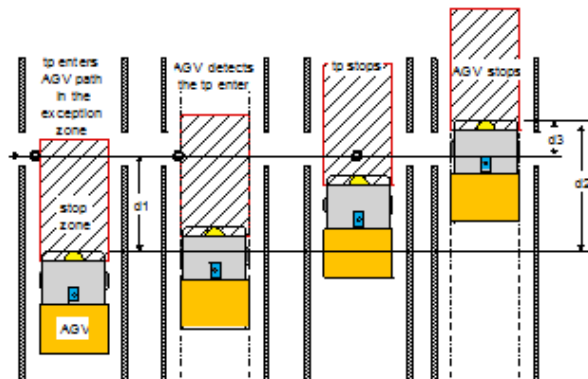


Figure 6 – Overhead view of the AGV and test piece positions for Test Method 2.

Parameter $d3$ therefore provides a comparison of the two braking methods, low-level emergency stop versus controlled braking.

Two pieces of information were captured from the tests: 1) comparison of braking distances for the two methods and 2) the energy reduced for the two different braking methods. Velocity versus distance travelled was plotted for all tests. Figure 7 shows plots from tests using the three AGV speeds, including: (a) 0.5 m/s, (b and c) 1 m/s, and (c) 1.2 m/s. Figure 7 (b and c) were separated

into two graphs for clarity. The points where the test pieces triggered Photosensor 1 are also indicated in Figure 9.

Tests 1 to 7, not shown, were tests where a static test piece was placed in the AGV path and the AGV stopping distance was checked to ensure that the current standard test method to ensure that the AGV stops prior to making contact with an obstacle was correctly followed. These tests showed that no contact was made using either braking method. The controlled braking tests allowed the vehicle to continuously measure separation distance and decelerate to a stop within a few centimeters of the test piece whereas the low-level emergency stop demonstrated a single stop was issued and produced an approximate 0.3 m separation distance to the test piece from the AGV when traveling at 1 m/s.

Figure 7 (a) shows comparison of the two braking methods at 0.5 m/s velocity for Tests 6 and 7. In this case, the braking distance is longer for the controlled braking

because the vehicle actually needed less than 2 m distance to stop and therefore decelerated at a rate that was appropriate for the vehicle speed. Figure 7 (b and c) shows results of Tests 9 to 19 for 1 m/s AGV velocity. Results clearly showed a difference in low-level stop and controlled braking with shorter stopping distance for controlled braking and which equates to a faster reduction in AGV kinetic energy.

Figure 7 (d) shows results of the tests with the AGV moving at 1.2 m/s. These test results show that the velocity stays at about 1.2 m/s for some time before there is a sudden drop in velocity, i.e., there was a delay in reaction. In these tests, results showed that controlled braking may have slightly higher reduction in energy, although the data plots are not very conclusive to determine the best braking method.

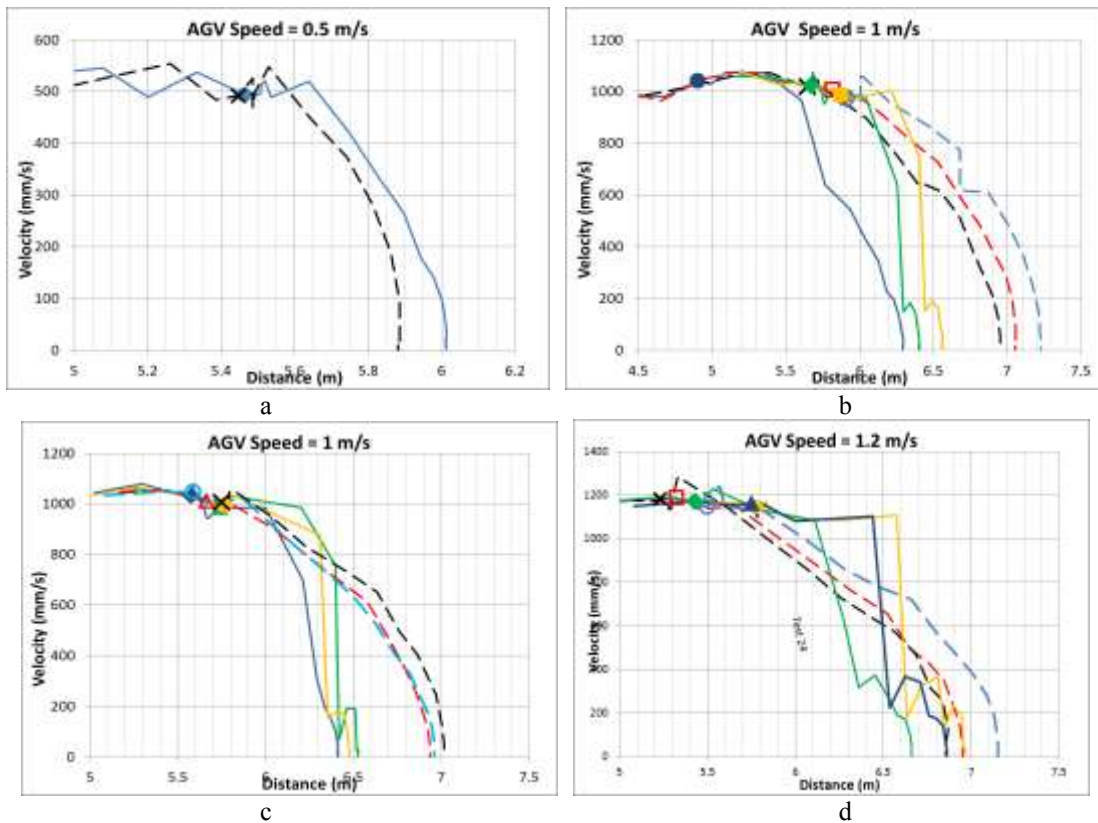


Figure 7 – Grid test results showing plots of AGV velocity versus distance for AGV velocities of: (a) 0.5 m/s, (b and c) 1 m/s, (d) 1.2 m/s. In these plots, solid lines show controlled braking and dashed lines show low-level stop. The various markers indicate when the test pieces entered the AGV path.

Potential sources of the delay in reaction may be due to:

- mechanical issues (e.g., time lag) from when the safety sensors detects the test piece to when the brakes are applied,

- software issues where the AGV controller computes a deceleration such that there appears to be enough time to stop and therefore does not apply the brakes until later
- or a combination of these two potential sources of error.

Static tests proved that the vehicle could detect, at 1.2 m/s programmed velocity, a static test piece in the AGV path and stop within the 2 m stop zone programmed into the safety sensor. Therefore, the safety sensor most likely detected the test piece. Further tests are required to determine the exact source of error.

Table 1 – Controlled braking versus low-level emergency stop

1 m/s tests		
Avg 1 m/s low lev d3	Avg 1 m/2 cnt brak d3	difference
0.72	0.23	68%
2 m/s tests		
Avg 2 m/s low lev d3	Avg 2 m/2 cnt brak d3	difference
0.71	0.56	22%

Table 1 shows a summary of parameter d3 results for tests with AGV velocities of 1 m/s and 1.2 m/s. Results clearly show that a reduction in distance, and therefore reduced AGV energy, is higher for controlled braking versus low-level emergency stop when the vehicle coasts to a stop. Electrical or mechanical braking could be used to stop the vehicle during an emergency stop and may also greatly reduce the energy similar to controlled braking. Coasting to a stop can also represent the typical braking distance required for a heavy industrial AGV and demonstrates that this braking method is not variably controlled to ensure payload stability or cause other potential benefits.

2.2.4 Method 2 Ground Truth

Ground truth for the locations of the test pieces along the grid was obtained using a computer image-processing approach and the same laser-based measurement system described in section 2.1.

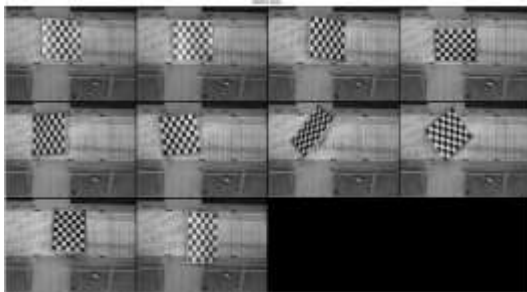


Figure 8 – Ten images of a checkerboard pattern placed within the camera’s field-of-view used for calibrating the camera’s intrinsic parameters.

The computer image processing phase used images captured from the overhead video by extracting the images that were manually identified (as described in Section 2.2.2) as the instances when the test piece first enters the AGV’s path (Figure 5 a) and when the test piece stops moving (Figure 5 c). The captured images were then corrected for distortions caused by the camera’s lens using a lens distortion model that was derived through a camera calibration routine. This routine involved taking pictures of a checkerboard pattern in various orientations within the camera’s field-of-view (see Figure

8) and then processing those images through a series of camera calibration algorithms to obtain the camera's intrinsic parameters (i.e., lens distortion).

Next, the images showing the test pieces were undistorted using the intrinsic parameters obtained as described above and then the images were transformed into the local coordinates of the laser-based measurement system. The transformation parameters between the undistorted camera images and the local coordinate system were determined by first measuring thirty-eight locations within the printed grid using the laser-based measurement system. The same grid locations were then manually selected in one of the camera's images in order to obtain their pixel coordinates. Using the two corresponding sets of 2D coordinates a projective transformation was found between them using a computer algorithm.

Finally, the positions of the test pieces were determined. For example, a circle with the same diameter as the cylindrical test piece was visually centered (in the image) on the circular part of the test piece (see Figure 9).

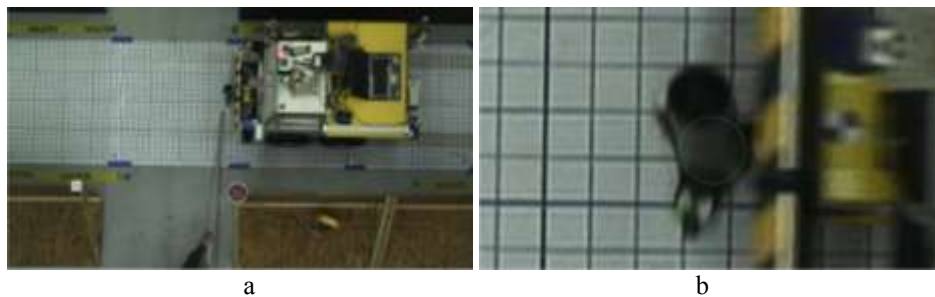


Figure 9 – The process of visually fitting a circle to the bottom of the test piece cylinder (a. overall view, b. close-up view of the test piece).

The coordinates of the center of the circle correspond to the coordinates of the center of the test piece on the printed grid in the local coordinate system.

The ground truth coordinates of the test pieces for all tests were determined using the method described in this section. These coordinates, along with the corresponding ground truth coordinates of AGV (obtained from the laser-based measurement system) at the instant when the test piece crossed the photo-sensor and when the AGV stopped, were projected onto the midline of the printed grid (along its long, or X, axis). The distances d1, d2 and d3 were then calculated as described in Section 2.2.2.

Table 2 –Errors in d1, d2 and d3.

	Average Error (cm)	Standard deviation of Error (cm)
d1	-5.4	8.1
d2	-4.3	6.6
d3	1.1	3.1

Table 2 shows the averages and standard deviations, for all the dynamic tests, of the errors for d1, d2, and d3, where the error is equal to the difference between the distances obtained using the video grid-based and ground truth methods. The results show that the video grid method can be used to calculate distances between the test piece and the AGV (along the X axis) of the grid with an error of between 4 cm and 6

cm of the actual (ground truth) distance. However, the standard deviation is very large indicating large variability in the calculated distances. Some sources of error include:

Video method

- Visual selection of frame. If the selection of the frame was off by one, the difference in distance would be about 3 cm based on an AGV velocity of 1 m/s and video frame rate of 30 Hz.
- Visually estimating location within a 5 cm x 5 cm square

Ground truth

- Camera intrinsic and extrinsic calibration errors
- Instrument error
- Measurement of the grid points
- Manual alignment of circle to bottom of cylinder in determining D1
- Grid paper misalignments, printing

Table 3 shows the average values for d3 calculated from the ground truth measurements for the tests in which the AGV was travelling at 1 m/s and 2 m/s. In Table 3, the d3 distances are sorted for the tests in which the AGV was stopped using either the low-level stop or controlled braking. In addition, the differences between the d3 values during the low-level stop and controlled braking tests are shown as a percentage reduction in distance travelled.

Table 3 – d3 values for low-level stop vs. controlled braking based on ground truth measurements.

Average d3 at 1 m/s		
Low Level	Controlled	Difference
72.0 cm	13.9 cm	80.7%
Average d3 at 2 m/s		
Low Level	Controlled	Difference
68.0 cm	54.4 cm	21.5%

Test Method 2 proved useful for measuring that the test piece did enter the exception zone and that controlled braking was better than low-level stop for 1 m/s AGV speeds. At a minimum, reduced energy was evident for both methods when the test piece entered the exception zone. Therefore, NIST recommends that ANSI/ITSDF B56.5 modify the current language for this clause to reflect this fact. Language could be included to require that the manufacturer show, through tests similar to test method 2, that the test piece

did enter the stop zone and that at various speeds the energy was reduced to a safe level.

3 Overhanging Obstacles

The current ANSI/ITSDF B56.5: 2012 standard states that obstacles must be measured throughout the contour area of the vehicle including any onboard equipment and payload. Figure 10 shows a typical arrangement of 2D LADAR imagers mounted on an AGV and configured to measure the AGV contour area as the AGV moves forward. As shown in the figure, there are large regions within the contour area that are not visible

even though there are four 2D sensors. With the rapid advancements of 3D imaging systems, replacing or augmenting the 2D sensors with one 3D imaging system could be feasible. Additionally, the use of a 3D imaging system could greatly reduce the regions not in the field of view of any sensor.

Research of 3D imaging sensors for use on AGV's is ongoing at NIST [3, 12] and in other organizations [13] [14]. Figure 11 shows the test pieces used in experiments reported in this paper: (a) stationary black flat plate positioned above the floor and in front of a ladder that is overhanging (i.e., the bottom of the ladder is not in the AGV path but the upper portion is in the AGV path) the AGV's path, (b) side view of the overhanging plate, and (c) a dynamic mock forklift tine, overhanging the AGV path.

The plate and tine were painted a flat black color to minimize signal return to imaging sensors – a conservative case. The overhanging obstacles shown in Figure 11 will not be detected by Sensor 3 (see Figure 10). They may be detected by Sensor 1 (see Figure 10) but the detection may not be soon enough for the AGV to stop without hitting the obstacle. A combination of controlled braking and Sensor 1 may however reduce the vehicle energy. The overhanging obstacles may be detected by the vertical scanning sensors labeled 2 and 4 in Figure 10.

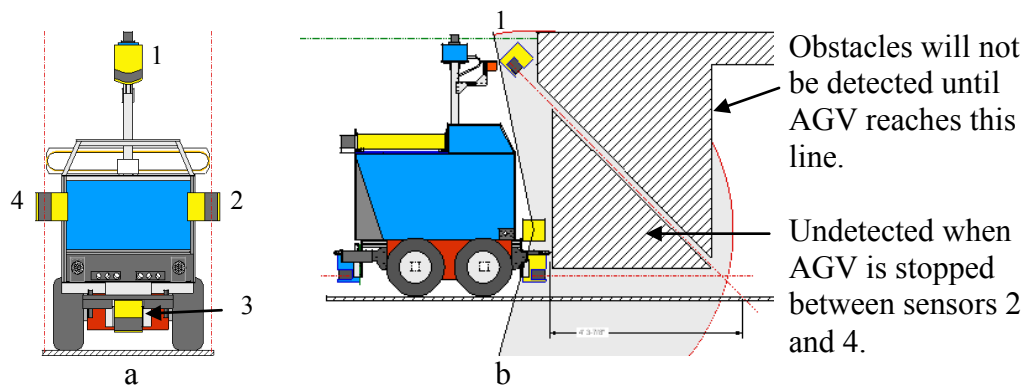


Figure 10 – Graphics showing (a) front and (b) side views of the NIST AGV with four front 2D safety sensors and the undetected regions. The red lines depict the planar regions sensed by the 2D sensors. The gray arc depicts the sensed areas from the vertically-mounted sensors. The undetected region includes a top region that is never detected by the sensor and therefore, extends indefinitely.

To determine if a vertical scanning LADAR can indeed detect the overhanging obstacles, such a sensor was mounted on the NIST AGV in the approximate location shown in Figure 10 (a) sensor #2 and is the blue sensor shown in Figure 11 (c). The sensor was connected to the controlled braking input of the AGV controller so that it could brake when an obstacle was detected. The results showed that the sensor detected the moving forklift tine, the static overhanging ladder, and plate when the plate was placed in-line with the sensor, and that the AGV stopped before contacting the obstacles. However, in industry, the plate may not be in the sensor's FOV and therefore may be undetected unless a sensor with a wider FOV or a 3D sensor was used.

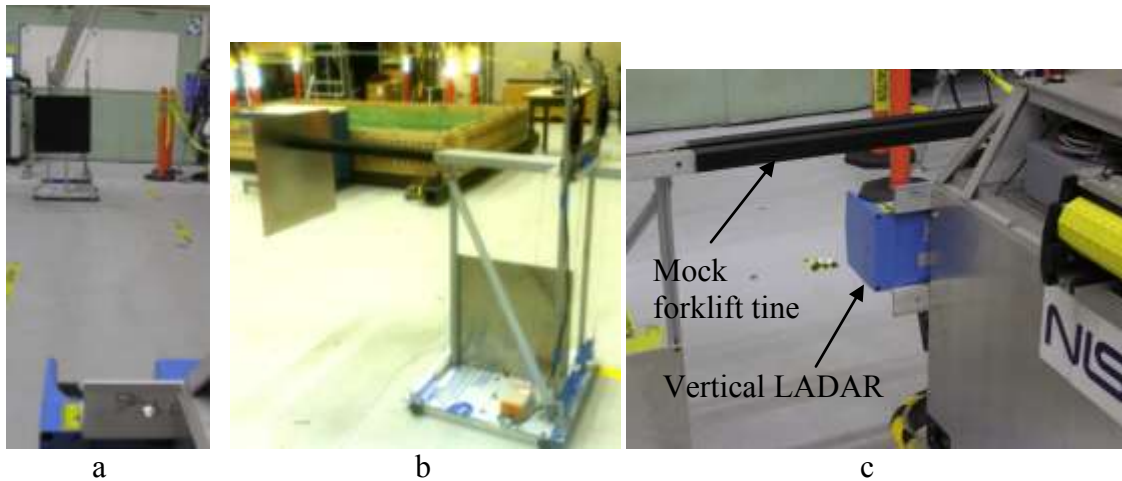


Figure 11 – View of (a) black flat plate from the front (b) flat plate from the side, and (c) mock forklift tine overhanging the AGV path. Both a and c are viewed from just behind the vertical LADAR.

In addition to the vertical LADAR, two different types of 3D imaging sensors were mounted on the AGV. Three flash LIDAR 3D imaging sensors were mounted on the AGV (see Figure 1). The three sensors were positioned to detect regions in front of the vehicle. The other type of 3D imaging sensor was a Kinect sensor as shown in Figure 3. None of the 3D sensors were connected to the vehicle controller; they were only used to collect data during the Method 1 experiments.

Figure 12 a, b, and c show some results from one of the flash LADAR and Figure 12 d, e, and f show results from a 3D Kinect sensor detecting the static overhanging plate. For these experiments, the AGV was moving at 1 m/s. Figure 12 also shows that floor-based obstacles can be detected.

In Figure 12 (a - c), the results were obtained from the center, top sensor and the sensor detected the plate at all ranges with the range from the AGV to the plate decreasing from Figure 12 (a) to Figure 12 (c). Figure 12 (a) shows the plate as a blue rectangle and Figures 12 (b and c) show the plate as a red rectangle; the color in Figure 12 is based on range with red indicating objects closer to the vehicle. Results from the two other 3D LIDAR sensors are not included in this paper because they were set to detect regions to the side of the AGV. The Kinect sensor results in Figure 12 (d - f) also detected plate and even the ladder behind the plate. Neither sensor would be sufficient, based on their limited FOV's, to detect the entire AGV contour region at a distance or very close to the vehicle and therefore, a combination of these sensors must be required.

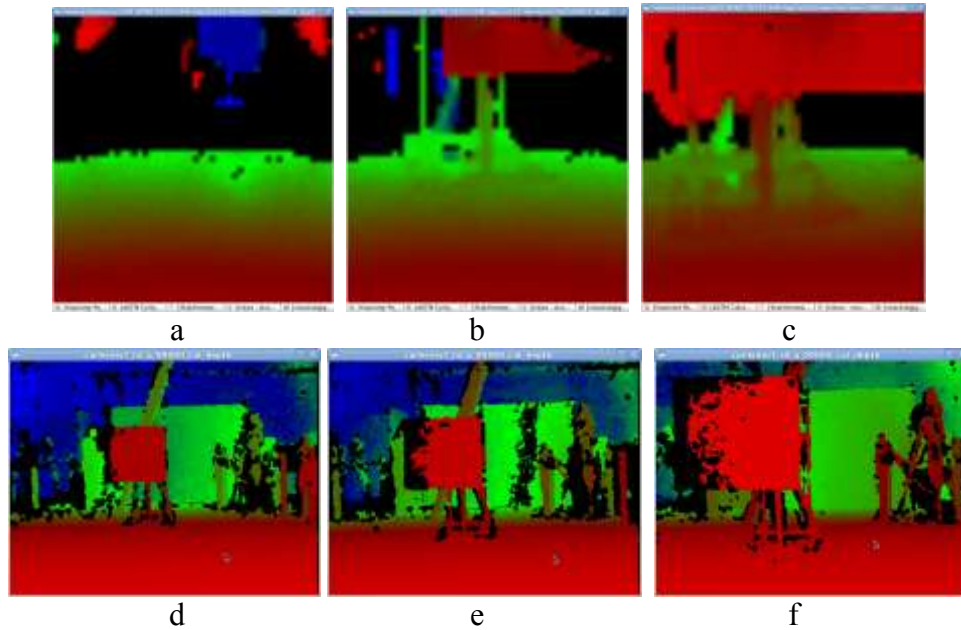


Figure 12 – Snapshots of data collected with (a, b, c) the 3D LIDAR sensor and (d, e, f) the Kinect sensor of an overhanging black plate statically positioned in the AGV path. Note the overhanging ladder in the background across the AGV path in the Kinect data.

4 3D Measurements of Dynamic Test Pieces

As mentioned earlier, measurements were taken simultaneously using 3D LIDAR and a Kinect sensor during the dynamic tests. Figure 13 shows snapshots of the AGV path when the test piece, a shiny flat plate, slid in front of the AGV within the stop zone. Figure 14 a, b, c shows results from a 3D LIDAR sensor: (a) before the test piece entered the zone, (b) when the test piece was in front of the vehicle, and (c) as the test piece exits the path showing the (red) vertical posts supporting the sensors for the ground truth instrument. Similarly, Figure 13 d, e, f show results from the Kinect sensor: (d) when the test piece is just entering the zone, (e) when the test piece was in front of the vehicle, and (f) as the test piece exits the path showing the (red) vertical ground truth detector posts. Based on Figure 12, a shiny, flat plate is detectable by a 3D sensor.

Similarly, an overhanging black mock forklift tine was attached to the sled and pushed into the AGV path. The vertical scanning LADAR detected the tine and stopped the vehicle prior to contacting it. 3D data were collected using the LIDAR and the Kinect sensors during these tests.

Figure 14 shows snapshots of the Kinect sensor data and clearly shows the tine entering the AGV path. The 3D LIDAR sensor data showed similar results.

Figure 15 shows (a) a photo of a mannequin in the AGV path; (b) 3D Kinect snapshot of the mannequin; (c) a photo of a mannequin after being detected by the vertical scanning LADAR; (d, e) 3D imaging sensor data from a 3D LIDAR sensor and (f, g) the Kinect sensor of the mannequin entering the AGV path. In the dynamic tests, the

mannequin was pushed into the AGV stop zone where the mannequin's right knee entered the path first and was detected with enough time to stop the vehicle using controlled braking without making contact with it.

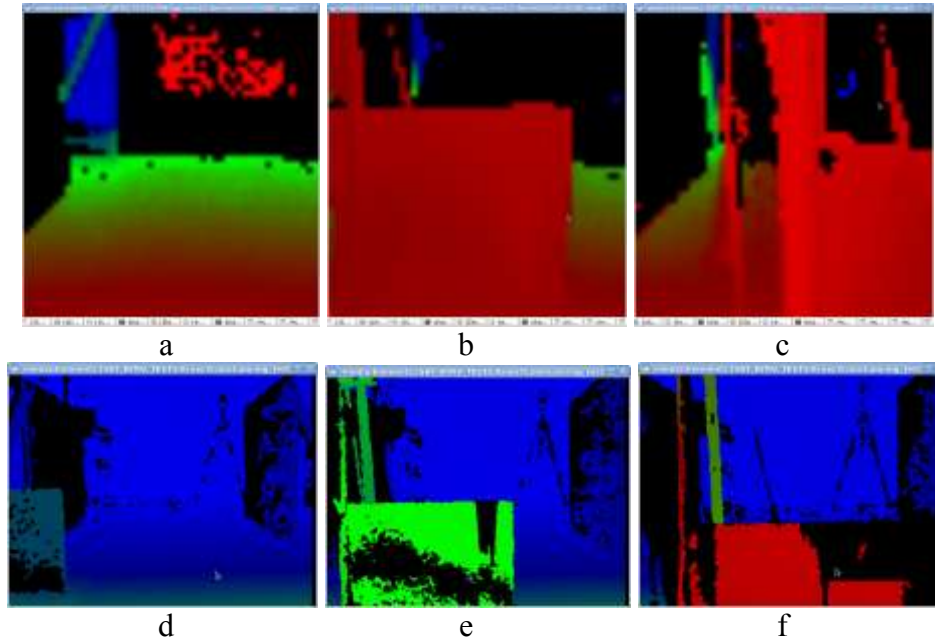


Figure 13 – Snapshots from (a, b, c) 3D LIDAR and (d, e, f) 3D Kinect sensors of the standard shiny flat plate test piece passing from left to right across the AGV path during the dynamic tests. Note the color changes of the test piece as it gets closer to the AGV signifying different ranges from the sensor.

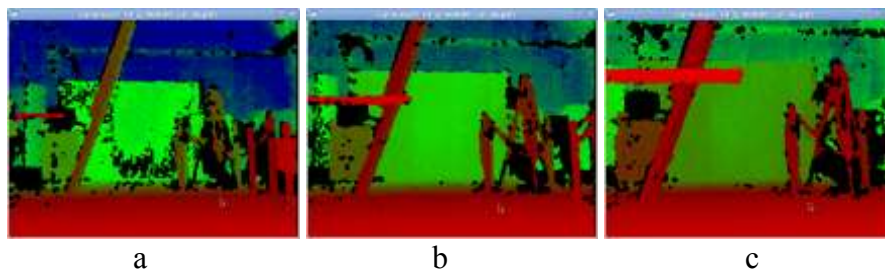


Figure 14 – Snapshots of data collected from the Kinect sensor of a black, mock forklift tine entering the AGV path. Note the overhanging ladder in the background crossing the AGV path.

The experimental data collected from 3D sensors on an AGV show that these devices can be useful for detecting obstacles in the AGV's path. However, research is needed on the use of 3D sensors to detect obstacles and to signal the AGV to slow or stop.

Advanced 3D imaging sensor technology used in our experiments may also prove useful for manned industrial vehicles by providing the operator with alerts to slow or stop the vehicle when obstacles are located in occluded regions. NIST has performed research

using 3D sensors mounted on a forklift to provide the operator with alerts. Figure 16 (top-left) shows a forklift backing up and nearing a piece of equipment and (bottom-left) shows the operator alert light turned on to indicate the region from which the alert originated. For these tests, a rear, downward-looking sensor and a rear-facing 3D sensor were used to obtain the data and an algorithm was developed to issue an alert.

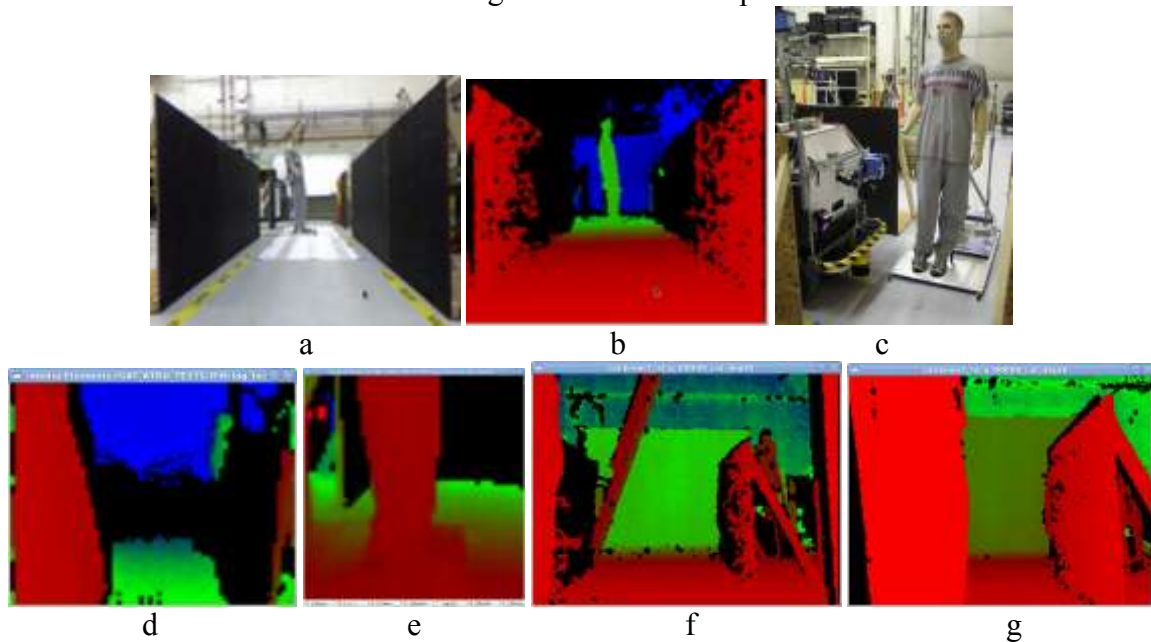


Figure 15 – (a) Photo of a static mannequin in the AGV path; (b) 3D Kinect snapshot of the static mannequin; (c) stopped AGV prior to contact with a mannequin that was pushed into the AGV stop zone; (d, e) 3D imaging sensor data from a 3D LIDAR sensor and (f, g) the Kinect sensor of the mannequin entering the AGV path.

An onboard computer computed in real time that an obstacle was in the vehicle's path and provided an output to an operator alert light. Figure 16 (right) shows the results of using a sensor mounted on the forklift tine frame to detect high or elevated objects. The 3D image (Figure 16 lower right) shows data when the sensor detected ceiling joists. It also shows green floor regions where there are no obstacles in vehicle path.

The research results in this section show that 3D imaging sensors can detect static and dynamic objects, on the ground or overhanging, that are in the path of a vehicle and enable the vehicle to stop without hitting the object. Although these sensors are not safety rated, they show potential for use on AGVs. It would be expedient for the ANSI/ITSDF B56.5 standard committee to develop test methods that can be used by all AGV manufacturers and users in anticipation of the time when these sensors are safety rated and broadly used.

Some suggested modifications to the ANSI/ITSDF B56.5 language to include 3D sensors would be:

- static, overhanging, standard test pieces must be detected at the same distance as the current static, ground-based test pieces;
- dynamic standard test pieces must also be detected when they enter the contour area of the vehicle path, regardless of whether they are overhanging or not, and prior to contact with the vehicle;
- obstacles that enter the exception (stop) zone of the AGV must be detected and it must be shown that the vehicle energy is reduced to a safe level as determined by the committee;
- Although 3D sensors are not yet safety rated, AGV non-contact safety sensors may be augmented by 3D sensors to provide improved obstacle detection.
- manned powered industrial vehicles may improve detection of obstacles within occluded regions by using non-contact safety sensors and/or by using 3D sensors that are not safety rated.



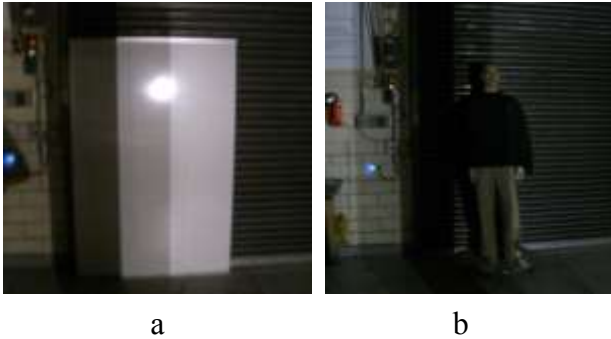
Figure 16 – (top-left) 3D LIDAR sensors mounted on a forklift and integrated with simple operator alerts. The obstacle is behind the forklift and (bottom-left) the alert indicates the location of the obstacle relative to the forklift, (right) high-lift obstacle detect sensor mounted on the forklift frame and raised (upper right inset photo is shown reversed from the data) to capture data of the ceiling joists.

The ideal situation would be if 3D imaging sensors were safety rated. Therefore, it would be advantageous if the sensor industry could provide 3D safety rated sensors for the AGV industry as it would expand the market for such sensors.

5 Manned Vehicle Visibility

5.1 Current Standard

The current ANSI/ITSDF B56.11.6 standard, soon to be called B56.11.6.1, includes a test method that uses a row of lights positioned where a forklift operator's head would be and shadows cast by the lights on a test board marked with a grid pattern. The shadows are



a b
Figure 17- Shadows: (a) on a test board as specified in the standard, (b) using a mannequin instead of the test board.

equivalent to occluded regions and are quantified by counting the grid blocks. Figure 17 (a) shows a standard test using a forklift and (b) a mannequin placed in the same shadowed region. The current method shows that there are occluded regions but does not specify their exact locations. Occlusion is caused by vehicle obstructions. Advanced imagers could be mounted to detect obstacles/pedestrians in these occluded regions. The current light method provides only the direction having occluded regions and not the

positions on the forklift where sensors might be mounted.

5.2 Advanced Detection of Obstacles in Occluded Regions

Advanced 3D imaging systems, for example stereo vision, LIDAR and LADAR sensors, along with high performance computers and software algorithms, can more accurately, than using the light/shadow method, characterize the regions occluded from the operator's viewpoint in a manned vehicle. Manufacturers can use this information to locate onboard sensors and to determine the type of sensor and the FOV required. The onboard sensor information could then be used to alert a forklift operator of a pedestrian crossing the vehicle path and to slow/stop the vehicle if necessary.

To demonstrate how an advanced 3D imaging system could be used to characterize the



Figure 18 – (left) forklift with scanner located at the operator's head location and (right) data plot from the scanner showing (black) occluded regions.

occluded regions in a forklift, such a system was located at the approximate position of an operator's head according to visibility standard test methods inside a forklift. A 360° (H) by about 320° (V) scan was performed. The set-up time was about 15 minutes and the scan time was about 5 minutes. The 3D point cloud is shown in Figure 18. The black regions are shadows cast by obstacles (e.g., cab frame) where the operator would not be able to see. In this demonstration, the forklift was unloaded. Further tests will be

performed using a laser scanner. Algorithms will be developed to quantify the sizes of occluded regions. Advanced pedestrian detection will be tested using 2D and 3D sensors.

Additionally, operator alerts and semi-autonomous control of the forklift will be demonstrated addressing the B56.5 automated functions of manned industrial vehicles.

5.3 Suggested modifications to ANSI/ITSDF B56.11.6

Currently, there is no discussion in ANSI/ITSDF B56.11.6 that describes other, advanced visibility test methods. Since the committee is harmonizing ANSI/ITSDF B56.11.6 with ISO/FDIS 13564-1 [15] and should they wish to add clause 8 “Other test methods” from ISO 13564-1, NIST suggests some modifications to this clause. In its current form, this clause may be incorrectly interpreted and may cause conflicting outcomes and/or other issues of visibility measurement tests. The clause is repeated here for the convenience of the reader:

“Other test methods (such as alternate light recording, cameras, computer imaging, lasers, etc.) may be used to conduct the test provided the alternate method duplicates the test with lights and produces the same results as the light method.”

The following are reasons for suggesting the changes:

- The “other test methods (such as alternate light recording, cameras, computer imaging, lasers, etc.)” is actually a series of ‘technologies,’ not test methods, and therefore, the clause as written is incorrect. The list also does not describe combinations of technologies that could potentially produce the same or better results than the light method. In addition, the other test methods could be a combination of the light method and a method that includes other technologies (e.g., cameras).
- Potential misinterpretation of the technologies is evident. The word “laser” can be interpreted as 1) a laser as a light source in place of the lamp as described in the standard, or 2) a laser-based 3D imaging system (e.g., laser scanner) which emits laser light and uses time-of-flight range measurement to detect objects in the environment, i.e., to measure visible and non-visible objects as seen from by the operator.

Given the two interpretations, appropriate text is needed for clarification. Also, if the second interpretation were allowed, the phrase, “produces the same results as the light method,” cannot occur with a scanning or flash LADAR (laser detection and ranging) system.

We assume the text: “same results as the light method” specifies the overall percentage of occluded regions for each test and therefore, we also include it in the proposed improvement. However, it may be clearer to the reader to include the text: “as shown in clause 10.2.1 and Table 3 (ISO/FDIS 13564-1).”

- “Computer imaging” should be replaced with the more well known “image processing.”
- The text: “duplicates the test with lights,” can be interpreted as the test must include the use of lights, possibly even using the same lights as detailed in the standard. No

additional lights are required for scanning or flash LADAR systems and therefore, this text should be removed.

A new clause 6 Other Test Methods has been proposed by NIST to the ANSI/ITSDF B56.11.6.1 based on past experience with advanced measurement systems at NIST [16] 17]. The new clause is based on ISO/FDIS 13564-1 clause 8 Other Test Methods. However, the proposed wording corrects the clause and provides more specific information with regard to the type of technology being used, including recording technologies used with the current light method and 3D imaging technologies. To help the reader better understand the proposed addition of a new clause 6, the following are examples of how the proposed “Other Test Methods” could be performed.

Proposed change:

6.1 Recording technologies

Other test methods that use recording technologies such as light recording or cameras and halogen lamps or alternate light sources such as light emitting diodes or lasers may be used to conduct the test provided these methods duplicate the standard test procedures in clauses 4 and 5 and produce the same results as the light method.

Example measurement and analysis method when using Cameras:

Measurement method 1: Lighting equipment, as defined in clause 3, using test procedures that adhere to clauses 4 and 5 with shadows captured using a camera that images the entire test object.

Analysis method 1: Image processing is used to determine light (visible) or dark (occluded) regions for each test.

Measurement method 2: An array of cameras is used instead of an array of lights as defined in clause 4.4 Light Source Array. The test procedures adhere to clauses 4 and 5 with visible test object areas captured using the array of cameras.

Analysis method 2: Image processing is used to determine visible regions of the test object for each test.

Proposed change:

6.2 3D imaging technologies

Other test methods that use 3D imaging technologies (such as laser scanners), computer modeling, and virtual test objects may be used to conduct the test provided these methods duplicate the standard test procedures in clauses 4 and 5, where the 3D imaging systems replace the halogen lamps, and produce the same results as the light method.

Example measurement and analysis method when:

Using 3 Dimensional (3D) Imaging from the Operator Cab:

Measurement method: A 3D imaging system (e.g., laser scanner) is used to measure 3D spatial information and positioned at each light origin according to clauses 4 and

5. (Note: it is possible that data do not need to be collected from all light origins, but a subset may be sufficient. For example, three locations instead of 13 locations along the light bar may be sufficient.) This information is then used to create a 3D visibility model from the vantage point of the vehicle operator. In a computer simulation environment, place a virtual test object and the 3D visibility model relative to each other according to clauses 4 and 5. Create a list of each light location for each test according to clauses 4 and 5.

Analysis method: Use a ray casting method on a computer to perform the following:

- a. Set the origin of the ray at a light origin.
- b. Project uniformly spaced rays onto the virtual test object.
- c. Repeat steps a and b for all light locations for that test.
- d. Calculate the light and dark regions according to clauses 4 and 5.
- e. Report the test results.

Using a Virtual Test Environment and 3 Dimensional (3D) Imaging

Measurement method: A 3D imaging system (e.g., laser scanner) is used to measure 3D spatial information about the vehicle (e.g., from several locations within the operator cab and external to the vehicle). This information is then used to create a 3D model of the vehicle. In a computer simulation environment, place a virtual test object and the 3D vehicle model relative to each other according to clauses 4 and 5. For each test, create a list of each light location according to clauses 4 and 5.

Analysis method: Use a ray casting method on a computer to perform the following:

- a. Set the origin of the ray at a light origin.
- b. Project uniformly spaced rays onto the virtual test object.
- c. Repeat steps a and b for all light locations for that test.
- d. Calculate the light and dark regions according to clauses 4 and 5.
- e. Report the test results.

6 Advanced Prediction of Obstacles

Both unmanned and manned powered industrial vehicles could benefit from knowing that a pedestrian or obstacle is approaching the vehicle path. Several technologies are available on the market, including for example, on and off-board vehicle cameras, LADAR, radio frequency identification (RFID), and ultra wideband (UWB) sensors. RFID and UWB sensors allow non-line of sight detection of obstacles.

Planned research at NIST will include evaluating the performance of RFID systems in the prediction of obstacles approaching the AGV and semi-autonomous forklifts paths. This information will be used to slow or stop the vehicle. The RFID non-line of sight capability is ideal for tracking moving obstacles anywhere in the laboratory and augments the line-of-sight sensors discussed earlier in this paper.

7 Conclusions

The NIST Mobile Autonomous Vehicles for Manufacturing Project evaluated automated guided vehicle (AGV) control based on 2D laser imaging safety sensors that can detect static and dynamic, standard test pieces representing humans and manufacturing equipment. Experiments and results were presented. Both controlled braking and low-level emergency braking control, as described in ANSI/ITSDF B56.5, were tested. Results showed that both braking methods reduced vehicle energy as standard test pieces moved into or were placed in the AGV path and within the exception/stop zone. In particular, the controlled braking method decelerated and stopped the vehicle within a shorter distance than the low-level stop method (coasting to a stop). This indicated that the energy transferred to an obstacle would be less for the controlled braking method than for the low-level stop method.

Two methods, Methods 1 and 2, were used to determine the performance of an AGV when an obstacle entered the AGV's path within the stop zone. Both test methods can be used to determine reduced energy as a function of controlled braking or low-level stop. Method 1 involved the use of onboard vehicle information from the navigation and safety sensors, but results did not correlate well with those from a reference instrument. Method 2 was developed to avoid using onboard vehicle information and therefore, would be easier for the AGV industry to implement. Method 2 involved the use of a video camera and a paper grid. Preliminary results show that Method 2 is a viable method, would be easier to use, and the results correlated well with those from a reference instrument. Further research will be performed to refine Method 2. This Method can then be used to generate the data needed to support recommended improvements to the stopping distance exception language in AGV standards.

Various 3D imaging sensors were used to detect overhanging obstacles. The tests showed that overhanging obstacles could be detected by the 3D sensors – even a low cost 3D sensor. These results show promise for the use of these advanced sensors on AGV's. Suggested changes to ANSI/ITSDF B56.5 to allow the use of 3D imaging sensors were presented.

A demonstration of possible visibility measurements was performed using advanced 3D imaging technology on a forklift. Proposed changes to ANSI/ITSDF B56.11.6 were described including examples of how potential tests methods could be performed.

Future NIST efforts related to the safe control of AGVs and forklifts in manufacturing environments include:

- tests using low reflectivity test pieces located next to similarly-colored walls,
- additional overhanging obstacle tests with AGV control based on 3D imaging sensor data, and
- radio frequency identification to predict pedestrian intent to enter the AGV path.

8 Acknowledgements

The authors thank the AGV manufacturers and SICK sensor manufacturer for providing their industry experiences.

9 References

- [1] ANSI/ITSDF B56.5 -2012 "Safety Standard for Driverless, Automatic Guided Industrial Vehicles and Automated Functions of Manned Industrial Vehicles."
- [2] ANSI/ITSDF B56.11.6-2005 "Evaluation of Visibility from Powered Industrial Trucks"
- [3] Roger Bostelman, Will Shackelford, "Time of flight sensors experiments towards vehicle safety standard advancements," Computer Vision and Image Understanding special issue on Time of Flight Sensors, 2010.
- [4] Roger Bostelman, Will Shackelford, Geraldine Cheok, Richard Norcross, "Standard Test Procedures and Metrics Development for Automated Guided Vehicle Safety Standards," Performance Measurement of Intelligent Systems (PerMIS) 2012, College Park, Maryland, March 2012.
- [5] Roger Bostelman, "White Paper: Towards Improved Forklift Safety," Proceedings of the 2009 Performance Metrics for Intelligent Systems Workshop (PerMIS'09), NIST Special Publication 1112, September 2009.
- [6] Roger Bostelman, Will Shackelford, "Performance Measurements Towards Improved Manufacturing Vehicle Safety," Proceedings of the 2009 Performance Metrics for Intelligent Systems Workshop (PerMIS'09), NIST Special Pub. 1112, 2009.
- [7] Roger Bostelman, Li Peng Liang, "Measurement and Evaluation of Visibility Experiments for Powered Industrial Vehicles," NIST Internal Report #7837, 2011.
- [8] Nikon iGPS, http://www.nikonmetrology.com/large_volume_tracking_positoining
- [9] Roger Bostelman, Will Shackelford, "Test Report on Highly Reflective Objects Near the SR3000 Sensor, NIST Internal Report to Consortium CRADA, 2008.
- [10] UL 61496: 2002 "Electro-Sensitive Protective Equipment Standard"
- [11] EN 61496-1, 2: 1997 "Safety of machinery: Electro-Sensitive Protective Equipment Standard"
- [12] Bostelman R., Hong T., Madhavan R., and T. Chang, "Safety standard advancement toward mobile robot use near humans," RIA SIAS 2005 4th International Conference on Safety of Industrial Automated Systems, Chicago, IL, 2005
- [13] Klas Hedenberg, Bjorn Astrand, "Safety standard for mobile robots - a proposal for 3D sensors," ECMR 2011.
- [14] D.D. Regan and R.R. Gray, "Visually guided collision avoidance and collision achievement," Trends in Cognitive Sciences, 4(3):99-107, 2000.
- [15] ISO/FDIS 13564-1: 2011, Powered industrial trucks -- Test methods for verification of visibility -- Part 1: Sit-on and stand-on operator trucks and variable-reach trucks up to and including 10 t capacity."
- [16] Cheok, G. S., Saidi, K. S., Franaszek, M., Filliben, J. J., and Scott, N. A., "Characterization of the Range Performance of a 3D Imaging System," NIST TN 1695, National Institute of Standards and Technology, Gaithersburg, MD, May 2011.
- [17] Cheok, G., Juberts, M., Franaszek, M., and Lytle, A., "3D Imaging Systems for Manufacturing, Construction, and Mobility," NIST TN 1682, National Institute of Standards and Technology, Gaithersburg, MD, December 2010.